2018 25th International Lightning Detection Conference &
7th International Lightning Meteorology Conference
March 12 - 15 | Ft. Lauderdale, Florida, USA

Forecasting Lightning Cessation Using Dual-Polarization Radar and Lightning Mapping Array near Washington, D.C.

Nancy Holden, Omar Nava, and Charlton Lewis
Department of Engineering Physics
Air Force Institute of Technology
Wright Patterson AFB, OH
Nancy.Holden@afit.edu

William Roeder
45th Weather Squadron
Cape Canaveral Air Force Station, FL

***Abstract*—This study verifies the probabilistic lightning cessation model developed by Joseph Patton [2017] at Florida State University for use by the U.S. Air Force's 45th Weather Squadron at Cape Canaveral Air Force Station (CCAFS) and NASA Kennedy Space Center (KSC). The Washington, D.C. greater metropolitan area, which presents a climate different to that of central Florida, was chosen as the domain of study. Dual-polarization radar and Lightning Mapping Array data were used to track 47 isolated, warm season thunderstorms in the greater metropolitan Washington D.C. area. The algorithm incorporates the presence of graupel at four isothermal levels, maximum reflectivity, and composite reflectivity using a bootstrapped generalized linear model. The model was tested for the 95.0%, 97.5%, and 99.0% probability thresholds. Performance statistics show that the model revealed notable skill in the Washington, D.C. area, yet not to the desired level as indicated by the model's performance in central Florida.**

Keywords—dual-polarization radar, Lightning Mapping Array, lightning cessation, forecasting lightning

I. INTRODUCTION

The most dangerous periods for lightning-induced injury or fatality coincide with not just the first lightning flash, but also the last [Holle, 1998]. As a storm appears to be dissipating, the perceived lightning threat diminishes. Often this occurs prematurely, and outdoor activity is resumed before the lightning potential has fully dissipated. Miscalculations of the timing of lightning cessation has resulted in avoidable casualties.

A recent study by Patton [2017] investigated a new probabilistic strategy for predicting lightning cessation. His model was designed for use by the 45th Weather Squadron (45 WS) at Cape Canaveral Air Force Station (CCAFS)/Kennedy Space Center (KSC). The 45 WS utilizes lightning watches to forecast the potential for lightning with a desired lead-time of 30 min; these alerts prompt resource protection measures to ensure base safety and operational mission success. Once lightning is detected on station or if lightning is imminent, a lightning warning is issued, notifying base personnel and halting operations. Since there is not much skillful guidance for forecasting the end of lightning occurrence, after-the-fact analysis has shown that the 45 WS lightning warnings remain active too long. This is costly due to lost productivity of outside workers, which can delay preparation for space launch and eventually even the space launch schedule.

Patton's [2017] probabilistic approach sought to improve the timing precision of the last flash occurrence. This improvement would allow lightning advisories to be canceled sooner and with more confidence. Patton developed a generalized linear model (GLM) in the form of a best-fit logistic regression. The idea was to designate weights for radar parameters of statistical significance to generate probabilistic guidance for total lightning occurrence. A database of 148 isolated, warm season thunderstorm cases were used in his study. Congruent with recent lightning cessation studies by Preston and Fuelberg [2015] and Davey and Fuelberg [2017], dual-polarization radar and a three-dimensional lightning mapping system were employed. Additionally, similar radar parameters were tested, with an emphasis on identifying parameters in the Mixed-Phase (MP) region of the cloud. The MP region is defined as the region between the 0◦C and approximately -20◦C isothermal levels where supercooled water droplets, graupel, and ice crystals coexist [Preston and Fuelberg, 2015].

Non-Inductive Charging (NIC) theory focuses on the MP region, and NIC is deemed one of the most widely accepted electrification methods to date. NIC theory describes a process involving melting and temperature gradients associated with interactions among graupel, ice crystals, and supercooled water

droplets [Takahashi, 1978]. During the non-inductive electrification process, large scale separation of charged particles occurs due to gravity [Rakov, 2016]. Ice particles and supercooled water droplets are also mobilized within the cloud. Following the schematic in Fig. 1, these particles collide with individual graupel particles and retain the charge of the opposite species [Zhang et al., 1991]. Typically, ice crystals develop a positive charge, while the graupel exhibits a negative charge. Therefore, the MP region and the presence of graupel within it play a key role in the lightning electrification and subsequently lightning cessation processes.

Consequently, Patton's [2017] study focused on these components of NIC theory. He used the dual-polarization derived Hydrometeor Classification Algorithm (HCA) product to determine graupel presence at the -5ºC, -10ºC, -15ºC, and -20ºC levels. In addition, maximum reflectivity values at 0ºC as well as the maximum composite reflectivity values were incorporated into the GLM. A bootstrapped version of the GLM shortened the presently used 45 WS wait time of 15 min after the last flash for forecasting lightning cessation. This result was consistent for the 95.0%, 97.5%, and 99.0% probability thresholds. The recommended probability threshold was the 97.5% threshold since it provided the optimal balance of time savings and a low false alarm ratio.

A better understanding of how this model performs can be achieved by testing this method in a climate different to that of central Florida. This study will verify Patton's lightning cessation model on a set of isolated thunderstorm cases in and around the Washington, D.C. area. Evaluating and comparing the results of this model in the new environment will provide insight into the model's versatility and efficacy. Consistent results will lend credence to the model's effectiveness and build confidence in the 45 WS's use of the method operationally. With significant positive results, these findings may even contribute to the eventual implementation of a similar algorithm in the Next Generation Radar (NEXRAD) radar network. Model discrepancies will also provide valuable information by exposing model vulnerabilities in a climate different to that of central Florida.

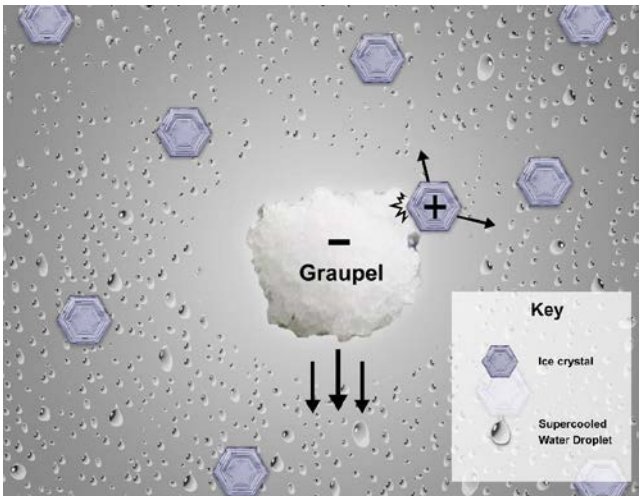

Fig. 1. Conceptual schematic of the NIC. Graupel particles interact with ice crystals in the presence of supercooled water droplets within the MP region.

II. DATA AND METHODOLOGY

A. Data

Patton's GLM was tested utilizing four dual-polarization Weather Surveillance Radar, 1988, Doppler (WSR-88D) radars from the National Weather Service in and around the Washington, D.C. area. The primary and preferred radar, based on its proximity to the domain of study, is located in Sterling, VA (KLWX). The three alternate radars are located in Dover AFB, DE (KDOX), College State, PA (KCCX), and Norfolk/Richmond, VA (KAKQ).

In addition, the New Mexico Tech Washington, D.C. Lightning Mapping Array (DCLMA) network was used to collect archived lightning flash data for each of the thunderstorm cases. The Lightning Mapping Array (LMA) network functions similar to the Second Generation Lightning Detection and Ranging (LDAR-II) network [Poehler and Lennon, 1979; Maier et al., 1995; Roeder, 2010] located at KSC and used in Patton's [2017] study. Patterned after the LDAR-II system, the New Mexico Tech LMA pinpoints the location of radiation using a GPS-based time of arrival technique to locate sources of very high frequency radiation. Multiple stations are utilized to identify lightning channels in three-dimensional space. This allows both intra-cloud (IC) flash channels and cloud-to-ground (CG) upper channels to be captured in addition to CG strikes [Rison et al. 1991; Krehbiel et al. 2000].

An initial database of 135 warm season thunderstorm cases from 2012-17 was acquired using the DCLMA archives for lightning data and the National Centers for Environmental Information archives for Level-II and Level-III radar data. These thunderstorm cases were further refined to 47 cases by using an event ranking system that established limiting criteria. Seven limiting criteria were selected for case elimination: cells with non-isolated, severe, or linear convective characteristics, cells exceeding an "effective distance" of 110 km from the radar and 100 km from LMA network, and poor health of the radar and LMA network. The spatial distribution of the final 47 cases is shown in Fig. 2.

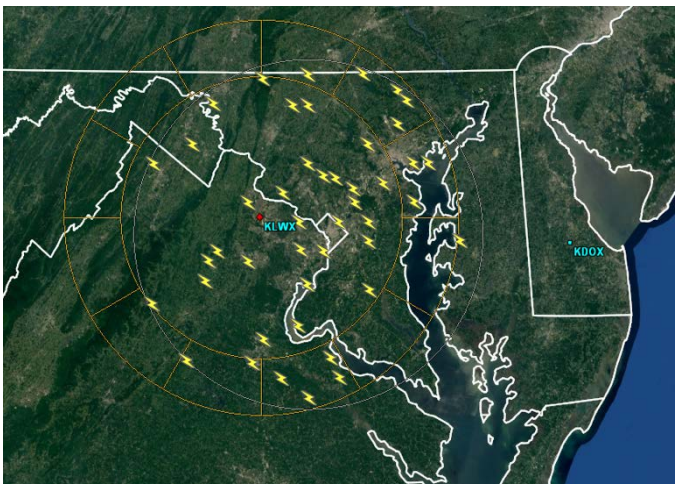

Fig. 2. Spatial distribution of the 47 isolated thunderstorm cases within the two designated LMA and KLWX radar range rings.

B. *Methodology*

Once a refined set of lightning cessation cases was collected, the time of lightning cessation, or the minute of the last recorded flash, was determined for each of the 47 cases. To ensure lightning flashes detected via the LMA network corresponded to the appropriate thunderstorm cell, hourly LMA images were used as a first glance comparison tool. Thereafter, MATLAB software [MATLAB, 2017] was used to pinpoint the precise time and location of the last lightning flash using the LMA data.

Each of the 47 lightning cessation cases were analyzed using the lightning cessation predictive model developed by Patton [2017]. Patton's recommended method for lightning cessation utilizes a bootstrapped GLM that incorporates six statistically significant predictor values (Table 1) and their corresponding coefficient values (Table 2). Predictor values at a specific time interval are input into the GLM equation given by Eq. 1 which generates the probability for lightning cessation at that time.

For this study in Washington D.C., thunderstorm cells were observed for a duration of 33 min, 16 min before and after observed lightning cessation. The storms were manually tracked at scanning intervals between 3 to 5 minutes, depending on the current radar Volume Coverage Pattern (VCP). At each time interval, radar parameters were collected at six isothermal levels: 0ºC, -5ºC, -10ºC, -15ºC, and -20ºC. These temperature levels were determined using Sterling, VA (KIAD) 00 UTC analyzed atmospheric sounding text data from the University of Wyoming's Atmospheric Science Department. The height corresponding to each isothermal level was recorded for each of the 47 cases. Since the height variation for each level was minimal (a maximum height variation of 2 kft), values for each isothermal height level were averaged. Furthermore, isothermal height levels were converted to isothermal layers for ease of manual analysis (Table 3).

TABLE I.

Level	Parameter (x_i)
Composite (maximum)	Maximum reflectivity (dBZ)
0°C	Maximum reflectivity (dBZ)
-5°C	Graupel presence (1 or 0)
-10°C	Graupel presence (1 or 0)
-15°C	Graupel presence (1 or 0)
-20°C	Graupel presence (1 or 0)

[a.] The six predictor radar parameters used in Patton's bootstrapped GLM [2017].

TABLE II.

Parameter (x_i)	Median Coefficient Value (c_i)
Maximum reflectivity (dBZ) at Composite	-0.2472
Maximum reflectivity (dBZ) at 0°C	-0.0637
Graupel presence (1 or 0) at -5°C	-1.1189
Graupel presence (1 or 0) at -10°C	-0.8548
Graupel presence (1 or 0) at -15°C	-0.8072
Graupel presence (1 or 0) at -20°C	-0.9997
Intercept (c_0)	16.0826

[a.] The six predictor coefficient values used in Patton's bootstrapped GLM [2017].

TABLE III.

Temperature levels	Isothermal Layers (ft.)
0°C	13,000-14,000
-5°C	14,000-18,000
-10°C	18,000-21,000
-15°C	21,000-23,000
-20°C	23,000-26,000

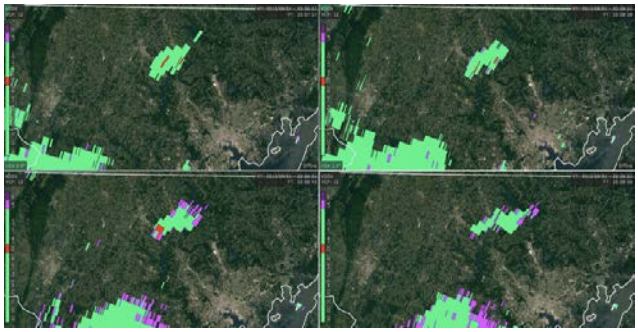

Fig. 3. KDOX radar image taken at 2206 UTC, prior to lightning cessation. HCA values displayed using GrLevel3 4-panel view, each panel showing a different elevation angle: 0.9º (top left), 1.5º (top right), 1.8º (bottom left), 2.5º (bottom right).

$$Probability(Cessation) = \frac{\exp(c_0 + c_1x_1 + c_2x_2 + c_3x_3 + \cdots)}{1 + \exp(c_0 + c_1x_1 + c_2x_2 + c_3x_3 + \cdots)} \quad (1)$$

Radar parameters were collected for each radar scan within the allotted time and grouped into 4-min bins. Tracking and analysis of radar data was done manually via GRLevelX software. Although manual analysis introduces the possibility of human error, storms were triple checked to ensure accuracy. Additionally, multiple radars were employed to ensure consistency and to fill in brief time gaps in radar data.

Predictor values incorporated into the GLM were extracted from dual-polarization radar data. Level-II and Level-III radar data downloaded from National Centers for Environmental Information (NCEI) were ingested and tracked manually via GRLevelX software. GRLevelX was developed by Gibson Ridge Software, LLC, and features a high-speed visual interface for radar data displayed on a high resolution radial grid (1 km x 1◦ x 230 km with 256 data levels). First, Level-III radar data was collected. GRLevel3 software was employed to analyze HCA and composite reflectivity values using a plan position

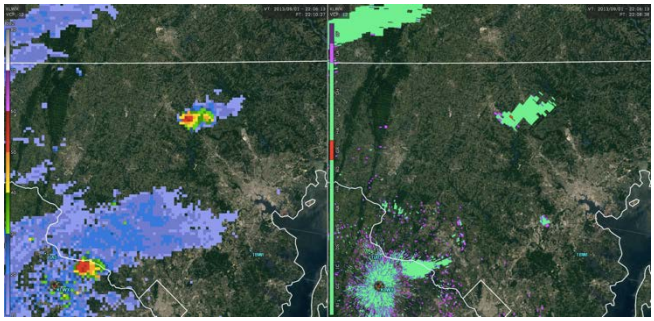

Fig.4. KDOX radar image taken at 2206 UTC, prior to lightning cessation. Composite reflectivity (left) and HCA (right) at the 3.5º elevation angle. Radar parameters displayed using GrLevel3 2-panel view.

indicator display. GRLevel3 offers a multi-panel viewing platform that was utilized for analyzing Level-III data quickly and efficiently. Fig. 3 displays an example four-panel view of HCA at four separate elevation angles using KDOX radar. Fig. 4 displays composite reflectivity and HCA at the 3.5° elevation angle using KLWX radar.

HCA values were analyzed at each available elevation angle. The required elevation angles were determined based on the estimated thermal layers listed in Table 3. The HCA color pallet was customized to facilitate the graupel identification process; graupel presence is represented by the bright red color as depicted in Fig. 3 and Fig. 4. The alternate radars (e.g. KDOX, KCCX, KAKQ) were employed to collect the remaining HCA data since the elevation angles for HCA using KLWX did not typically encompass the isothermal heights beyond -10°C. In this case, KDOX was used to identify graupel presence in the remaining three elevation angles required for analysis (Fig. 3).

After Level-III radar data was acquired, Level-II maximum reflectivity values at 0°C were collected. GR2Analyst software was used to visualize the data, and the cross-section feature was implemented to analyze the data. Fig. 5 shows the layout of the cross-section feature with height and horizontal distance displayed on the vertical and horizontal axes, respectively. Toggle buttons in the right panel under "position" and "swing" were utilized as tools to scan through each thunderstorm cell and pinpoint the maximum reflectivity value at the 0°C level.

Following analysis, 4-minute binned data were interpolated to 1-min intervals by adopting a cubic Hermite spline interpolation method. This method utilizes a piecewise, continuous function comprised of third order polynomials. Due to its piecewise construct, cubic spline interpolation prevents Runge's phenomenon, a manifestation of artificial oscillations in the function due to higher order polynomial interpolation. The interpolated value at a query point is based on a shape-preserving piecewise cubic interpolation of the values at neighboring grid points. Therefore, cubic spline interpolation allows for a smoother curve that is a better representation of what is observed in nature, while still maintaining its true shape.

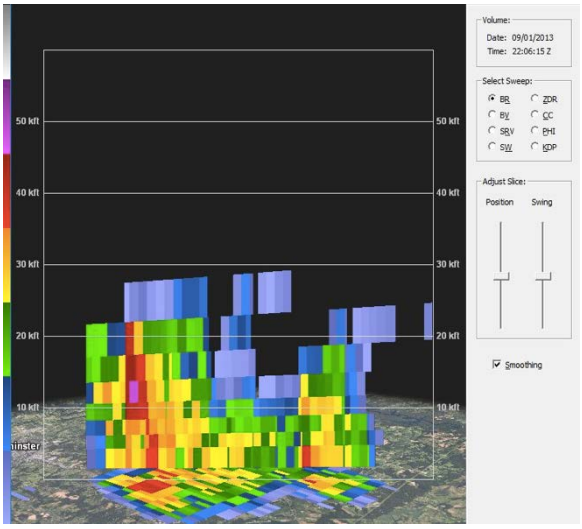

Fig. 5. Example GR2Analyst radar cross-section of reflectivity of a thunderstorm cell.

III. ANALYSIS AND RESULTS

Two approaches were used to evaluate the performance results and calculate the verification statistics of Patton's [2017] GLM in the Washington, D.C. area. The first approach ingests all 1,551 minutes of data, and then designates a forecast outcome for each minute/observation in accordance with Table IV. Probability thresholds were set to indicate that above these threshold values, the model predicted lightning cessation. Below these probability thresholds, lightning was predicted to still be ongoing. Three threshold probabilities were selected to match that of Patton: 95.0%, 97.5%, and 99.0%. These thresholds allow the model to be tested, and the performance metrics to be determined.

For the first approach, every minute observation was categorized as either a hit, miss, false alarm, or correct null in accordance with Table IV. A false alarm corresponds to the prediction of lightning cessation when lightning is still ongoing. This is the most dangerous case in terms of safety. A hit refers to an observation/minute which indicates lightning cessation is correctly predicted. In contrast, a miss refers to the event in which lightning cessation is not forecast, but lightning has already ended. Finally, the correct null refers to an observation that indicates lightning is ongoing, and the model correctly forbears the prediction of lightning cessation.

TABLE IV.

		Was cessation observed at this minute?	
		Yes	**No**
Was cessation forecast at this minute?	**Yes**	Hit	False Alarm
	No	Miss	Correct Null

Once the forecast metrics for the data were determined, a set of verification measures defined by Equations 2-6 were calculated. These measures were used to determine the skill of the model. Bootstrapped results established a 95% confidence interval depicting the performance statistics' variability. The Probability of Detection (POD), or hit rate, refers to the proportion of lightning cessation events that were correctly forecasted [Donaldson et al., 1975; Jolliffe and Stephenson, 2012] and is defined as:

$$Probability\ of\ Detection = POD = \frac{Hits}{Hits + Misses} \quad (2)$$

With regards to the POD, a value close to 1.0 is desired and conveys that there were minimal missed forecasts in relation to hit forecasts. This means the model is correctly detecting and predicting lightning cessation. It is important to note that the POD does not take into account the false alarms and should therefore not be used as the sole method for determining the skill of a forecast. The False Alarm Ratio (FAR) refers to the probability of a false alarm given that an event was forecast [Donaldson et al., 1975; Jolliffe and Stephenson, 2012]. In terms of lightning cessation, the FAR corresponds to the

probability of forecasting lightning cessation when lightning is still ongoing. The FAR is defined as:

$$False\ Alarm\ Ratio = FAR = \frac{False\ Alarms}{Hits + False\ Alarms} \quad (3)$$

FAR values range from 0.0 to 1.0. The ideal FAR is 0.0, signifying that the number of false alarms is limited. Similar to the POD, the FAR should not be used alone to measure the skill of a forecast due to the strong dependence on the number of hits. In this case, rare events will score higher than random forecasts of common events, and thus is deemed inequitable. In this study an equitable measure is one that gives all random forecasting systems the same score [Gandin and Murphy, 1992]. This provides a no-skill baseline against which a forecaster can be examined in contrast to have skill. While the use of FAR alone is inequitable, using FAR and POD conjointly can provide a more accurate measure of the skill of the model; a perfect skill score would have a FAR of 0.0 and a POD of 1.0. The POD values for all probability thresholds were significantly lower for the Washington, D.C. area compared to central Florida. Results show that POD values were not contained within the bootstrapped 95th percentile ranges (Fig. 6). However, the FARs for all probability thresholds corresponding to central Florida were contained within the error bars corresponding to the Washington, D.C. area. Therefore, although the model has a low POD for the Washington, D.C. area, low FARs reveal that the model tends to evade the most dangerous outcome by waiting until lightning ceases to safely predict cessation.

Heidke Skill Score (HSS) and True Skill Statistic (TSS) are verification measures that provide useful stand-alone performance statistics of the dataset. The HSS is a measure of the fractional improvement of the forecast over the standard forecast, chance [Jolliffe and Stephenson, 2012; Murphy and Daan, 1985]. This measure utilizes a performance variable, namely the Expected Correct (EXPCOR), that incorporates all possible forecast metrics as well as the total number of events. EXPCOR is defined as:

$$Expected\ Correct = EXPCOR = \frac{(Hits + Misses) * (Hits + False\ Alarms)}{Total\ Events} + \frac{(Correct\ Nulls + Misses) * (Correct\ Nulls + False\ Alarms)}{Total\ Events} \quad (4)$$

EXPCOR represents the number of forecasts expected to verify based on chance. HSS is defined as:

$$Heidke\ Skill\ Score = HSS = \frac{(Hits + Correct\ Nulls) - EXPCOR}{Total\ Events - EXPCOR} \quad (5)$$

The sum of hits and correct nulls in the numerator represents the number of times that the forecast matches the actual observation. HSS values range from $-\infty$ to 1.0; a perfect forecast would obtain a score of 1.0. Alternatively, random forecasts would be awarded a score of 0.0. The TSS, also known as the Peirce Skill Score, is a verification measure that takes all event outcomes outlined in Table 4 into consideration [Flueck, 1987; Jolliffe and Stephenson, 2012; Murphy and Daan, 1985; Peirce, 1884]. The TSS is defined as:

$$True\ Skill\ Statistic = TSS = \frac{(Hits * Correct\ Nulls) - (False\ Alarms * Misses)}{(Hits + Misses) * (False\ Alarms + Correct\ Nulls)} \quad (6)$$

TSS values range from -1.0 to 1.0 with a desired value of 1.0. For rare events, the number of correct nulls is large and TSS is weighted accordingly. Both TSS and HSS are considered truly equitable, and will output an expected score of zero for both random and constant forecasts. As equitable, stand-alone measures these statistics are the most valuable. Thus, they will be emphasized in this study.

The TSS values for all three probability thresholds for the Washington, D.C. area were approximately half the TSS values for central Florida (Fig. 7). Thus, the TSS values for the respective locations are statistically different. This confirms the model's discrepancies in geographically separated areas with differing climates. Nevertheless, there are a few promising results from this approach. The consistency between the HSS

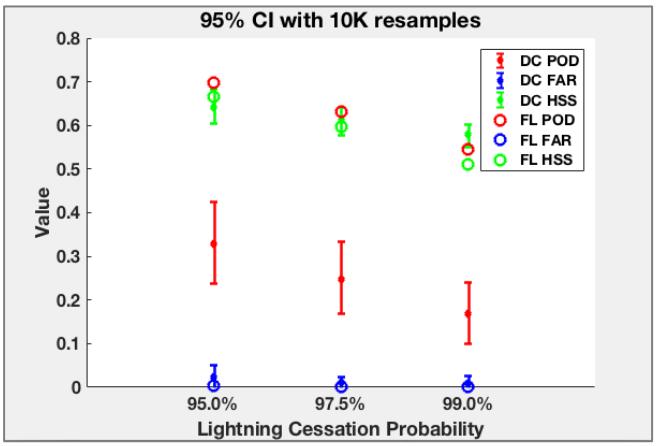

Fig. 6. POD, FAR, and HSS performance statistics for Patton's GLM in Washington, D.C. and central Florida. Washington, D.C. performance statistics and bootstrapped results utilizing the 95th percentile are depicted by the diamonds and error bars, respectively. Central Florida performance statistics are overlaid in circles.

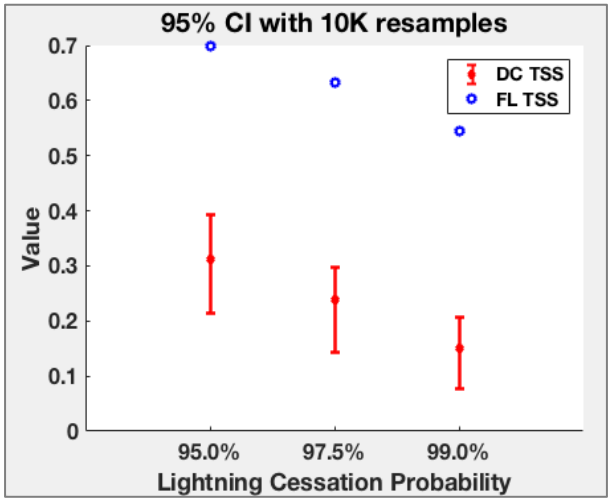

Fig. 7. TSS performance statistics for Patton's GLM in Washington, D.C. and central Florida. Washington, D.C. performance metrics and bootstrapped results using the 95th percentile are depicted by the blue diamonds and error bars, respectively. Central Florida performance statistics are overlaid in blue circles.

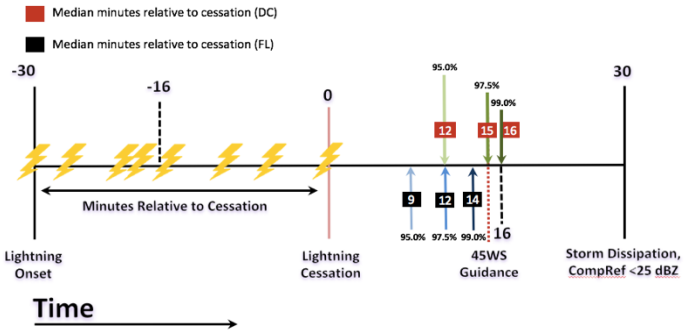

Fig. 8. Timeline depicting the conceptual 60-min lifetime of an isolated thunderstorm from lightning onset to storm dissipation (adapted from Patton [2017]). The solid red line at 0 minutes corresponds to the observed time of lightning cessation. The 16-minute markers prior to and following lightning cessation correspond to the storm observation window. The green and blue arrows represent the three probability thresholds from Patton's GLM for Washington, D.C. and central Florida, respectively. Similarly, the minutes in red and black blocks represent the median time relative to lightning cessation for Washington, D.C. and central Florida, respectively.

values in Washington, D.C. and central Florida indicates that the model does convey significant skill, and is more accurate than the standard forecast. The 95th percentile ranges from the bootstrapping validated these model consistencies for the HSS values (Fig. 6).

The second approach manages the data on a storm by storm basis, whereby the model is trying to successfully predict lightning cessation for each case. Fig. 8 presents a conceptual timeline of a thunderstorm case from storm initiation to storm dissipation. Each thunderstorm case is defined by a single metric: hit, miss, or false alarm. Hits, misses, and false alarms are all calculated based on strict time limits with respect to the observed time of lightning cessation. The objective is to correctly predict cessation within 1 to 15 minutes after lightning cessation is observed. This method tests the model's performance against the 45 WS's presently used wait time of 15 min. The correct null does not exist for this approach since lightning cessation is observed for every case. Thus, for this

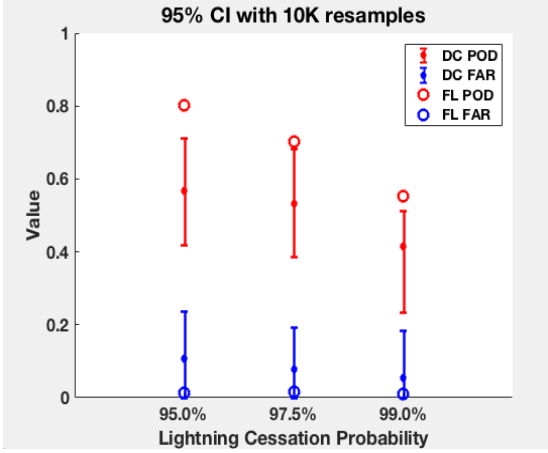

Fig 9. Storm by storm POD and FAR performance statistics for Patton's GLM in Washington, D.C. and central Florida. Washington, D.C. bootstrapped performance statistics utilizing the 95th percentile are depicted by the diamonds and error bars. Central Florida performance statistics are overlaid in circles.

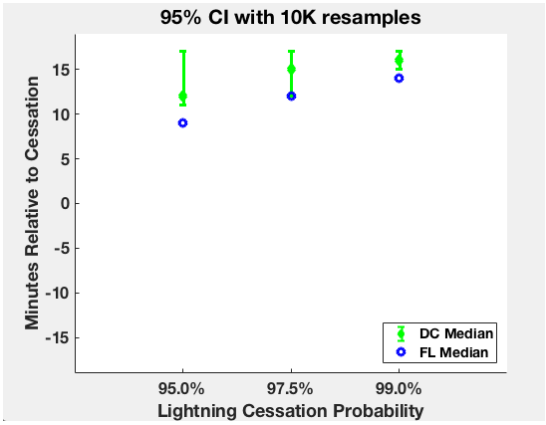

Fig 11. Median lag-times for Patton's GLM in Washington, D.C. and central Florida. Washington, D.C. bootstrapped results utilizing the 95th percentile are depicted by the green error bars and are overlaid with the results for central Florida in blue circles.

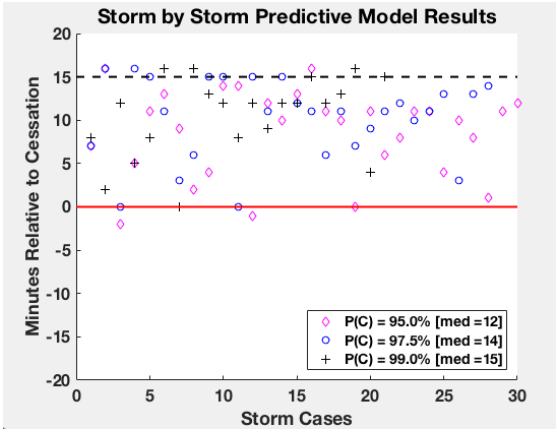

Fig. 10. Storm by storm lag-times for thunderstorm cases in Washington, D.C. Markers beneath the solid red line indicate false alarms, and markers above the dashed black line indicate that the model waited too long to predict lightning cessation (beyond the 45 WS wait time of 15 min). The total 47 cases are not displayed because the observation time was constrained to 16 min before and after lightning cessation.

approach there is no situation that yields a case outcome which correctly predicts the non-occurrence of lightning cessation.

Similar to the results of the first approach, POD values were lower for all probability thresholds for the Washington, D.C. area in comparison to central Florida (Fig. 9). The median wait times were also calculated to compare to the median lag-times determined in Patton's study. A 95% confidence interval was calculated using 10,000 resamples of the dataset to bootstrap the results. The median lag-times for Washington D.C. are 12, 15, and 16 min for the 95.0%, 97.5%, and 99.0% probability thresholds, respectively (Fig. 10 and Fig. 11). These median lag-times for the three probability thresholds in the Washington, D.C. area were all longer than the analyzed lag-times in central Florida. The 95.0% threshold was the most promising result, with a 12-minute lag-time after cessation compared to the 9-minute lag-time for central Florida. Though this result is significant, the FAR for the 95.0% threshold must also be considered, since it displayed the highest value over all thresholds: 2.4% and 10.7% using the first and second approach, respectively. While the more conservative probability

thresholds, 97.5% and 99.0%, convey no improvement from the 45 WS presently used 15-minute wait time, these thresholds do offer some utility by providing the forecaster greater confidence that lightning has truly ended.

IV. CONCLUSIONS

This research verifies the probabilistic lightning cessation guidance developed by Patton [2017] for the 45WS's use at CCAFS/KSC. To test the model's overall consistency and versatility in a climate different to that of central Florida, the GLM was tested in and around the greater metropolitan Washington, D.C. area. Using a dataset of 47 isolated thunderstorm cases from 2012-17, the DCLMA and dual-polarization radar were employed to test the model's performance.

The bootstrapped GLM utilizes six key dual-polarization radar predictor values: graupel presence at the -5◦C, -10◦C, -15◦C, and -20◦C isothermal levels, maximum reflectivity at the 0◦C level, and the maximum composite reflectivity. These predictor values give insight into the mechanisms that sustain lightning generation and the physical properties indicative of lightning cessation.

The results were evaluated using two approaches to verify the model's performance. The first approach considered every minute as an individual event with a singular outcome, while the second storm by storm approach considered each storm as an individual event with a singular outcome. Comparison of the performance statistics for the GLM in the Washington, D.C. area and in central Florida reveals that for both approaches Patton's GLM did not perform as well in the Washington, D.C. area as it did in central Florida. However, performance statistics show that the model did achieve skill and the 95.0% probability thresholds did shorten the wait time by 3 minutes, while still achieving statistically similar HSS values. Additionally, the storm by storm verification approach revealed that while the model performed worse in Washington, D.C. than central Florida, some of the performance statistics were still comparable and thus reassuring.

These findings indicate that key radar parameters utilized by the model were statistically significant for predicting lightning cessation for both locations. Specifically, graupel presence within the MP region plays a vital role in the lightning electrification processes according to NIC theory. Also, the use of isothermal temperatures levels as opposed to height levels are excellent coordinates for identifying radar parameters, since they have consistent properties regardless of geographical location. This corroborates the results of Patton [2017] and Preston and Fuelberg [2015] which identified graupel presence at specific isothermal level(s) as statistically significant. During analysis, graupel presence was almost always observed throughout the MP region during active lightning. Likewise, there was a noticeable trend in the rapid reduction of graupel presence promptly after observed lightning cessation. This decline in graupel presence started at the upper levels, and percolated to the lower levels with the successive minutes after cessation. This pattern complemented Patton's lightning cessation model well. However, the model still tended to delay the forecast of lightning cessation for too long. This can be attributed to the reflectivity trends of the Washington, D.C. storms. The storm reflectivity values tended to be too high for too long, causing the model to unnecessarily delay the prediction of lightning cessation.

Discrepancies in the model's performance can possibly be attributed to key climate differences for the two domains of study as well as methodology incongruities. With regards to climate, the difference in forcing mechanisms, airmasses, and the disproportionate concentration of aerosols in the environment convey key climate distinctions for the two locations. Washington, D.C. exhibits a greater population density compared to that of central Florida. This characteristic suggests that there are more anthropogenic aerosol emissions in Washington, D.C. compared to central Florida. This exposes the Washington, D.C. atmosphere to a different atmospheric particle composition capable of interacting differently with hydrometeors and altering cloud electrification mechanisms.

Furthermore, the difference in forcing mechanisms prevalent in the Washington, D.C. area compared to those prevalent in central Florida has significant impacts on lightning generation and cessation. Although both locations are situated along the coast, the latitudinal differences create different atmospheric environments for storm development. While central Florida is characterized as a more barotropic environment, the Washington, D.C. environment exhibits more baroclinic tendencies. Furthermore, Washington, D.C. is under predominantly continental air with westerly flow while central Florida is predominantly under maritime air with easterly and westerly flow. This key difference exposes Washington, D.C. to more frontal systems than central Florida. Subsequently, central Florida is exposed to more airmass thunderstorms due to sea breezes originating from both east and west coastlines. Selecting solely warm season thunderstorms aimed to avoid the baroclinic systems prevalent in spring and fall which typically foster more linear, multicellular, and severe thunderstorms.

Future work is required to corroborate the conclusions of this thesis and to clarify the discrepancies in the performance of Patton's [2017] lightning cessation predictive model in Washington, D.C. This includes repeating the process by automating the entire analysis process, increasing the number of thunderstorm cases by analyzing thunderstorms from other geographical locations, and testing different dual-polarization radar parameters. The results of this study suggest that the Patton [2017] method may be applicable in climates different from central Florida if tweaks were made to the predictor and coefficient values using a similar probabilistic GLM approach. To gain a deeper understanding of the model's comprehensive skill and performance, the Patton method should be tested in climates both similar and dissimilar to that of central Florida. Locations such as Alabama and Oklahoma which have active New Mexico Tech LMA networks are ideal locations for testing. While the LMA in Alabama is closer to the climate in central Florida, especially in summer, the LMA in Oklahoma would provide a test in a different climate. In addition, LMAs supporting field research could provide spot checks in additional climate scenarios.

In conclusion, although Patton's lightning cessation GLM did not achieve the same level of success in Washington, D.C. as it did in central Florida, the results were still promising.

Recommendations for action would be to retain the probabilistic guidance concept from Patton [2017] and develop and test various GLMs with a new combination of radar parameters extracted from the MP region. Ideally, thunderstorms from select locations across the nation would be incorporated into the storm database. This has the potential to achieve a more comprehensive lightning cessation predictive model, delivering skillful lightning cessation guidance for locations with differing climates.

ACKNOWLEDGMENT

This research was sponsored by the 45th Weather Squadron and the Engineering Physics Department under the Air Force Institute of Technology. I would like to thank my advisor Maj Omar Nava, and my committee members, Charlton Lewis and William Roeder for their mentorship and expertise.

REFERENCES

Davey, M. J. and Fuelberg, H. E. (2017). Using radar-derived parameters to forecast lightning cessation for nonisolated storms. J. Geophys. Res. Atmos., 122:3435–3456.

Donaldson, R., Dryer, R., and Kraus, M. (1975). An objective evaluator of techniques for predicting severe weather events. In Ninth Conference on Severe Local Storms, pages 321–326, Norman, OK. Amer. Meteor. Soc.

Flueck, J. (1987). A study of some measures of forecast verification. In Conference on Probability and Statistics in Atmospheric Science, pages 69–73, Edmonton, Canada. Amer. Meteor. Soc.

Gandin, L. and Murphy, A. (1992). Equitable scores for categorical forecasts. Mon Weather Rev., 120:361–370.

Holle, R. L., Lopez, R. E., and Zimmermann, C. (1999). Updated recommendations for lightning safety-1998. Bull. Amer. Meteor. Soc., 80(10):2035–2041.

Jolliffe, I. T. and Stephenson, D. B. (2012). Deterministic forecasts of binary events. In Forecast Verification: A Practitioner's Guide in Atmospheric Science, chapter 3, pages 31–59. John Wiley & Sons, Chichester, England, 2d edition.

Krehbiel, P., Thomas, R., Rison, W., Hamlin, T., Harlin, J., and Davis, M. (2000). GPS-based mapping system reveals lightning inside storms. Earth and Space Sci. News, 81(3):21–25.

Maier, L., Lennon, C., Britt, T., and Schaefer, S. (1995). LDAR system performance and analysis. In Proceedings of the International Conference on Cloud Physics.

Murphy, A. and Daan, H. (1985). Forecast verification. In Murphy, A. and Katz, R., editors, Probability, Statistics and Decision Making in the Atmospheric Sciences, pages 379–437. Westview Press, Boulder, CO.

Patton, J. R. (2017). Using radar-derived parameters to develop probabilistic guidance for lightning cessation within isolated convection near Cape Canaveral, Florida. M.S. Thesis.

Peirce, C. S. (1884). The numerical measure of the success of predictions. Science, 4(93):453–454.

Poehler, H. A. and C. L. Lennon (1979). Lightning Detection and Ranging (LDAR) system description and performance objectives. NASA Tech. Memo. 74106, 86 pp.

Preston, A. D. and Fuelberg, H. E. (2015). Improving lightning cessation guidance using polarimetric radar data. Wea. Forecasting, 30:308–328.

Rakov, V. A. (2016). Fundamentals of Lightning. Cambridge University Press.

Rison, W., Thomas, R. J., Krehbiel, P., Hamlin, T., and Harlin, J. (1999). A GPS- based three-dimensional lightning mapping system: Initial observations in central New Mexico. Geophys. Res. Lett., 26(23):3573–3576.

Roeder, W. P. (2010). The four dimensional lighnting surveillance system.Third Int. Lightning Meteorolgoy Conf., Orlando, FL, Vaisala.

Takahashi, T. (1978). Riming electrification as a charge generation mechanism in thunderstorms. J. Atmos. Sci., 35.

MATLAB version 9.2.0 (2017). The MathWorks Inc. Natick, Massachusetts.

Zhang, R., Williams, E. R., and Rydock, J. (1991). Mixed-phase microphysics and cloud electrification. J. Atmos. Sci., 48(19).